MATERIALS SCIENCE

Carbon-boron clathrates as a new class of sp^3-bonded framework materials

Li Zhu[1], Gustav M. Borstad[1]*, Hanyu Liu[1†], Piotr A. Guńka[1,2], Michael Guerette[1], Juli-Anna Dolyniuk[1], Yue Meng[3‡], Eran Greenberg[4], Vitali B. Prakapenka[4], Brian L. Chaloux[5], Albert Epshteyn[5], Ronald E. Cohen[1,6,7], Timothy A. Strobel[1§]

Carbon-based frameworks composed of sp^3 bonding represent a class of extremely lightweight strong materials, but only diamond and a handful of other compounds exist despite numerous predictions. Thus, there remains a large gap between the number of plausible structures predicted and those synthesized. We used a chemical design principle based on boron substitution to predict and synthesize a three-dimensional carbon-boron framework in a host/guest clathrate structure. The clathrate, with composition $2Sr@B_6C_6$, exhibits the cubic bipartite sodalite structure (type VII clathrate) composed of sp^3-bonded truncated octahedral $C_{12}B_{12}$ host cages that trap Sr^{2+} guest cations. The clathrate not only maintains the robust nature of diamond-like sp^3 bonding but also offers potential for a broad range of compounds with tunable properties through substitution of guest atoms within the cages.

INTRODUCTION

As a fundamental building block of nature, carbon is unrivaled in its diversity to form stable structures with other elements and itself. One-dimensional (1D) carbon-based materials (e.g., polymers) have thoroughly reshaped society over the past century, in addition to providing the building blocks for life. 2D materials (e.g., graphene and metal borocarbides) attracted attention due to remarkable properties potentially useful for advanced technology (*1*–*4*). The limited number of 3D sp^3 carbon-based structures includes diamond, lonsdaleite (a hexagonal diamond allotrope) (*5*), B-doped diamond (*6*), SiC (*7*), and BC_2N (*8*). These materials all have several attractive properties for applications that include hardness, strength, thermal conductivity, and electron mobility. Boron carbide also contains sp^3-hybridized carbon, but these atoms serve as dopants within or linkages between B icosahedra (*9*, *10*), rather than establishing the overall structural framework. Of broader interest are 3D covalent organic frameworks (COFs), which are formed by linking sp^2-hybridized molecular building blocks, that have attracted attention for gas storage and separations (*11*). Compared with the exquisite synthetic control over porous COF materials, the experimental progress in denser sp^3 carbon-based structures lags far behind.

Numerous 3D carbon allotropes and compounds are predicted to have feasible energies for synthesis and interesting properties (*12*). However, it remains unclear whether any of these materials can be produced in the laboratory. Aside from the diamond structure, almost no other sp^3 carbon-based frameworks are known or can be stabilized at atmospheric pressure. For example, longstanding predictions of 3D sp^3-bonded C_3N_4 networks have not been realized thus far (*13*), and high-pressure polymeric phases of CO_2, which consist of a network of CO_4 tetrahedra, decompose into molecular CO_2 phases when decompressed (*14*).

Another impressive 3D sp^3 material is the carbon clathrate. Carbon-based clathrates are open-framework structures composed of host cages that trap guest atoms, in which all host atoms are linked by four-coordinate bonds. As sp^3-bonded frameworks, carbon-based clathrates potentially represent strong and lightweight materials that also offer tunable properties through manipulation of the occupancy and type of guest atoms within the cages. Despite their prominence in other systems with tetrahedral coordination (*15*–*18*), carbon-based clathrates are tremendously challenging to synthesize. Attempts to synthesize carbon clathrates go back at least 50 years since they were postulated following the formation of inorganic silicon clathrates (*18*, *19*), and their possible structures and properties are of long-standing interest (*20*, *21*). Some proposed carbon clathrates are expected to exhibit exceptional mechanical properties with tensile and shear strengths exceeding those of diamond (*22*), while large electron-phonon coupling is predicted to give rise to conventional superconductivity with high transition temperatures (*23*, *24*). If produced, these materials would represent a class of diamond-like compounds wherein the electronic structure is tunable by adjusting the occupancy of electron-donating (or withdrawing) atoms within the cages (*25*).

A substantial amount of research has been performed to answer the persisting question of whether carbon clathrate structures are accessible by experiment. First-principles density functional theory (DFT) calculations indicate that both filled and guest-free carbon clathrates are energetically unfavorable, but by energies as low as 0.07 eV/atom relative to diamond (for reference, commercially produced C_{60} is metastable by nearly six times that energy) (*12*, *26*). Synthesis of carbon clathrates might therefore proceed through a nonequilibrium pathway (e.g., formation from a high-energy precursor or deposition method) or through a chemical substitution/doping strategy to modify the intrinsic thermodynamic stability.

[1]Geophysical Laboratory, Carnegie Institution for Science, 5251 Broad Branch Road, NW, Washington, DC 20015, USA. [2]Faculty of Chemistry, Warsaw University of Technology, Noakowskiego 3, 00-664 Warszawa, Poland. [3]High Pressure Collaborative Access Team, Geophysical Laboratory, Carnegie Institution for Science, Advanced Photon Source, Argonne, IL 60439, USA. [4]Center for Advanced Radiation Sources, University of Chicago, Chicago, IL 60637, USA. [5]Chemistry Division, U.S. Naval Research Laboratory, Washington, DC 20375, USA. [6]Department of Earth and Environmental Sciences, Ludwig Maximilians Universität, Munich 80333, Germany. [7]Department of Physics and Astronomy and London Centre for Nanotechnology, University College London, London, UK.
*Present address: Department of Physics and Materials Science, University of Memphis, Memphis, TN 38152, USA.
†Present address: State Key Laboratory of Superhard Materials and Innovation Center for Computational Physics Methods and Software, College of Physics, Jilin University, Changchun 130012, China.
‡Present address: HPCAT, X-ray Science Division, Argonne National Laboratory, Lemont, IL 60439, USA.
§Corresponding author. Email: tstrobel@carnegiescience.edu

The closest synthesized materials that have a structure only resembling a carbon clathrate are 3D polymers of C_{60} (*27*).

While nonequilibrium synthesis pathways remain feasible in concept, another strategy is to substitute boron for carbon atoms within the cage frameworks of carbon clathrates. The electron-deficient nature of boron creates the ability to form complex chemical bonding with itself or carbon to stabilize polyhedra, such as the icosahedral units in molecular carborane clusters (*28*, *29*). Zeng *et al.* (*30*) calculated that boron substitution improves the intrinsic thermodynamic stability of carbon clathrate frameworks. Nevertheless, no thermodynamically stable carbon-clathrate was predicted after examination of a small subset of possible B substitution schemes in Li-filled carbon clathrates. A broad search of potential B substitution schemes is needed to validate this chemical stabilization principle. We used automatic structure searching methods (*31*) to predict and then synthesize a thermodynamically stable carbon-boron sp^3-bonded clathrate.

RESULTS

We conducted an extensive search in the Sr-B-C system (Fig. 1A) at pressures from 0 to 200 GPa after broader searching in other ternary B-C systems (see Materials and Methods for additional information). For the Sr-B-C system, we determined that several high-pressure compounds are thermodynamically stable with respect to elemental mixtures (Fig. 1B). At 50 GPa, we calculated that the hexagonal $P6_3/mmc$ and γ-B structures are the most stable forms of Sr and B, respectively, while diamond is the most stable structure for C. We found the compounds Sr_5C_2, SrC, SrC_2, Sr_5C_2, SrB, SrB_2, SrB_4, and SrB_6 are stable binaries on the convex hull at 50 GPa. We found no energetically stable B-C binary compounds above 50 GPa, in agreement with a previous computational study (*32*).

We predicted two stable ternary compounds at 50 GPa. The first hexagonal SrBC ($P6_3/mmc$) exhibits 2D layers of six-membered B-C rings stacked between layers of Sr^{2+} cations, similar to intercalated graphite. This SrBC phase is isostructural with LiBC found at ambient pressure (*3*) and similar to other metal borocarbide phases with different ring tilings (*2*, *4*). The second ternary compound is cubic ($Pm\bar{3}n$) with composition $2Sr@B_6C_6$ (SrB_3C_3) and has the type VII clathrate structure, known for the clathrate hydrate $HPF_6{\cdot}6H_2O$ (*33*) and superhydrides such as $CaYH_{12}$ (*34*). The topology of SrB_3C_3 is that of bipartite sodalite (sod-b), which is distinguished from the sodalite structure (sod) in that carbon atoms are only bonded to boron atoms and vice versa.

The SrB_3C_3 clathrate framework (Fig. 2) is composed of a single truncated octahedral cage with six four-sided faces and eight six-sided faces ($4^6 6^8$). The cages are composed of 24 vertices with alternating C and B atoms, and each cage contains a single Sr^{2+} cation at the center. We predicted that this type VII clathrate phase is thermodynamically stable from 50 to at least 200 GPa at 0 K. The material does not exhibit imaginary phonon frequencies at any pressure indicating dynamic stability and a favorable structure for metastable recovery to ambient conditions. At zero pressure, the optimized lattice parameter is 4.88 Å, and the structure contains one unique B-C bond length of 1.73 Å. The boron-doped clathrate is much more stable than its pure carbon counterpart. At 50 GPa, $2Sr@C_{12}$ is metastable by 0.667 eV/atom, while $2Sr@B_6C_6$ lies on the convex hull.

Our DFT calculations show that at 50 GPa, SrB_3C_3 is a stable product of exothermic reactions of the pure elements and of readily accessible binary compounds. We therefore conducted diamond anvil cell (DAC) experiments using homogeneous fine-grained mixtures of SrB_6, SrC_2, and glassy C targeting the stoichiometric reaction $SrB_6 + SrC_2 + 4C \rightarrow 2SrB_3C_3$. We conducted additional experiments using only mixtures of binary compounds, where the most energetically favorable reaction we calculated was for $SrB_6 + 3SrC_2 \rightarrow SrB_3C_3 + 3SrBC$. We compressed mixtures of the powders in Ne or Al_2O_3 media and heated near ~2500 K using an infrared fiber laser, while synchrotron x-ray diffraction (XRD) patterns were collected to monitor structural changes in situ.

The starting SrB_6 has the LaB_6 ($Pm\bar{3}n$) structure, whereas SrC_2 takes on the acetylide structure of CaC_2 ($I4/mmm$). When compressed at room temperature, SrB_6 remains in the starting cubic phase, and SrC_2 transforms to the $R\bar{3}m$ structure above 14 GPa, eventually appearing amorphous above 50 GPa. Upon heating near 2500 K, the intensities of diffraction peaks from the starting compounds vanish, and a series of new reflections appear. At 57(3) GPa, we indexed these sharp lines to a phase-pure BCC lattice with $a = 4.5972(2)$ Å, in

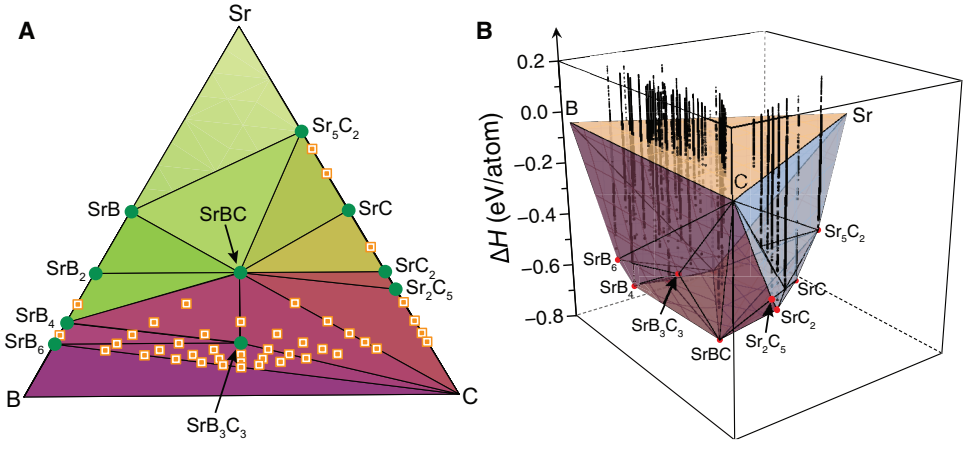

Fig. 1. Stable compounds in the Sr-B-C system. (**A**) Ternary phase diagram at 50 GPa. Green circles represent thermodynamically stable compounds, while orange squares represent metastable compositions used in the search. (**B**) Ternary convex hull for the Sr-B-C system at 50 GPa based on formation enthalpies. Compounds with enthalpy data represented by red points are on the convex hull and thermodynamically stable against decomposition. Black points show the formation enthalpies of metastable structures found in the structure searches.

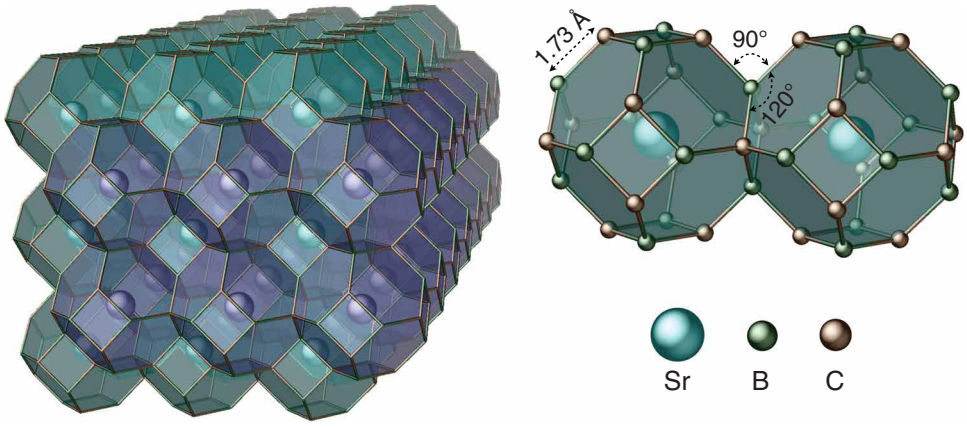

Fig. 2. Structure of SrB_3C_3 clathrate. The cubic structure ($Pm\bar{3}n$) is composed of face-sharing boron-carbon cages that encapsulate Sr^{2+} cations. Each cage contains 24 atoms with six four-sided faces and eight six-sided faces ($4^6 6^8$). Different color cages are used to emphasize the stacking of cages that tile 3D space.

excellent correspondence with the type VII SrB_3C_3 clathrate ($Pm\bar{3}n$) with a calculated lattice parameter of $a = 4.593$ Å at the same pressure.

We compared the calculated XRD pattern of the SrB_3C_3 clathrate with experimental scattering data (Fig. 3A). Given the nearly complete experimental powder averaging statistics, the quantitative diffraction intensities are representative of atomic positions and are in excellent agreement with the calculated pattern of SrB_3C_3 clathrate to the experimental resolution limit of 0.75 Å. All allowed reflections with appreciable intensity are observed to this limit, consistent with the formation of SrB_3C_3 clathrate.

Given the large contrast in electron density between Sr and the framework atoms, the heavier element dominates the intensity of scattered x-rays. While the formation of SrB_3C_3 is strongly supported by the stoichiometric conversion of the starting materials and agreement with the calculated stable structure, the intensities of the allowed reflections that differentiate the primitive bipartite structure from the BCC sodalite version are minimal, and it is challenging to confirm the clathrate structure on the basis of powder XRD alone. By annealing a sample at high-pressure and high-temperature conditions [56(4) GPa, ~3000 K], we were able to produce crystalline grains suitable for single-crystal diffraction. Single-crystal diffraction offers a more decisive characterization of the unit cell because it includes 3D geometrical relationships in addition to *d* spacings. Analysis of the data confirms the sp^3-bonded framework and allows us to unambiguously determine the clathrate crystal structure, exhibiting the symmetry of the $Pm\bar{3}n$ space group. Structural models for the ordered bipartite structure are better than other models for the C/B framework (table S1). Furthermore, the formation of the clathrate phase is confirmed by the experimental *P-V* equation of state, which uniquely distinguishes clathrate cage structures based on agreement with DFT calculations over a broad pressure range from 0 to 150 GPa (Fig. 3B). SrB_3C_3 and other higher-energy cage variants are much less compressible than all other stable and metastable elemental structures and binary/ternary compounds calculated except pure boron allotropes and diamond (fig. S1). Energy-dispersive x-ray spectroscopy measurements performed on a recovered sample exhibiting the cubic XRD pattern are also consistent with the formation of SrB_3C_3 clathrate near this composition (fig. S2).

The SrB_3C_3 framework exhibits strong covalent bonding between sp^3-hybridized B and C atoms and weak interactions with the Sr^{2+} guest. This strong sp^3-hybridized covalent framework guarantees a high value for the bulk modulus [experimental $B_0 = 249(3)$ GPa] and incompressibility of SrB_3C_3 clathrate. The estimated Vickers hardness for the SrB_3C_3 clathrate, based on calculated elastic properties, is 24 GPa, comparable with the hardness of tungsten carbide (*35*). On the basis of electron count, SrB_3C_3 should be a hole conductor, and calculations show that it is. All-carbon, four-coordinate zeolites are insulators at low pressures as closed-shell systems analogous to diamond. A sodalite all-carbon clathrate fits in this class, as does isoelectronic $[C_3B_3]^{3-}$. SrB_3C_3 is one electron per formula unit short of this magic (insulator) electron count. The calculated band structure (Fig. 4) shows a good gap for one electron more than SrB_3C_3.

DISCUSSION

SrB_3C_3 clathrate is likely the first member of a new class of strong and lightweight sp^3-bonded carbon-based frameworks with tunable properties. Because boron anions are isoelectronic to carbon atoms in the B-C framework, the bipartite structure should also exhibit exceptional properties due to the similar nature of bonding in hypothetical pure carbon cages. SrB_3C_3 clathrate is calculated to be conducting, and samples exhibit a metallic luster. The electronic band structure (Fig. 4B) shows the coexistence of steep and flat bands close to the Fermi level (near the M point), which sets favorable conditions for superconductivity (*36*). Thus, SrB_3C_3 is a candidate for phonon-mediated superconductivity at ambient pressure. Furthermore, the ability to trap various kinds of guest atoms in the sp^3-bonded cages allows the carbon-based clathrates to exhibit diamond-like mechanical properties with a tunable electronic structure. While SrB_3C_3 is metallic, the electronic structure may be modified by substituting different guest atoms. For example, LaB_3C_3, which we also predict to be thermodynamically stable at high pressure, has a band gap due to the balanced electron count. The removal of guest ions from the cages offers an additional space to explore the possibility for guest-free structures (*37*). Although SrB_3C_3 is only thermodynamically stable at high pressure, we recovered it at atmospheric pressure, similar to diamond. At 1 atm, SrB_3C_3 persists when kept under an inert atmosphere. The clathrate degrades when exposed to the moisture in air over a few hours. The clathrate we discovered provides a platform for investigating other substitutions of the framework or guest atoms. More broadly, using boron to stabilize carbon frameworks may be applicable to entirely different structure types.

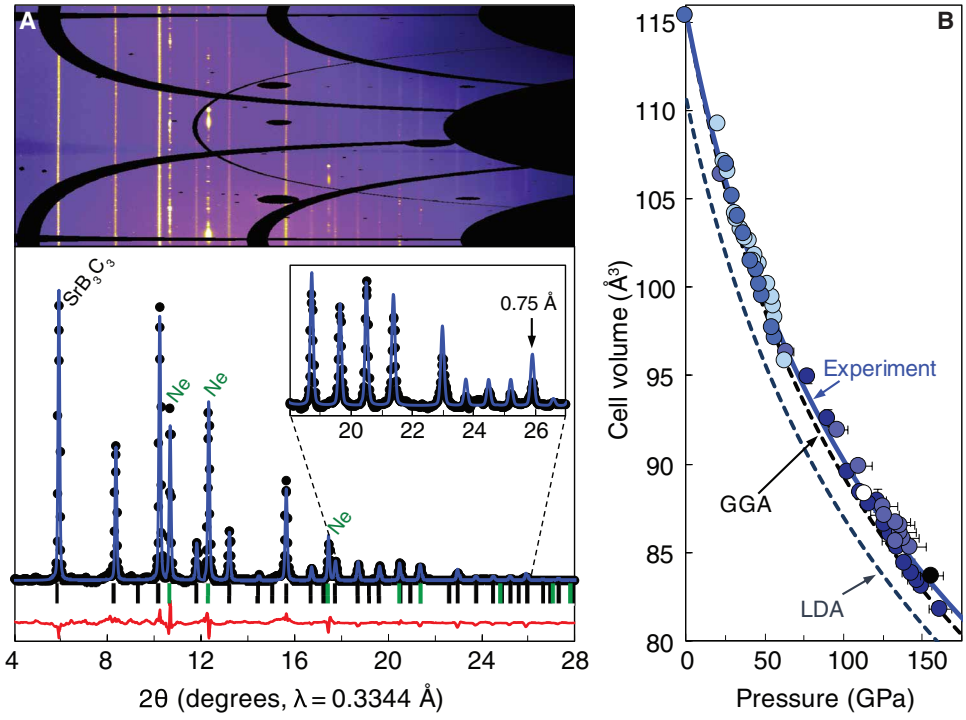

Fig. 3. XRD and equation of state of SrB_3C_3. (**A**) Experimental XRD data (black points) collected at 57(3) GPa with Rietveld refinement (blue line) of the SrB_3C_3 phase. Green ticks indicate contributions from Ne with Le Bail refinement. The 2D diffraction ("cake") aligned with the integrated pattern shows nearly complete powder averaging with sharp peaks for the SrB_3C_3 phase. Black regions on the detector image indicate nonintegrated ("masked") regions due to diamond anvil reflections and features of the detector. The inset shows a magnified view at high angle with sharp SrB_3C_3 peaks to a limiting resolution of 0.75 Å. (**B**) Experimental third-order Birch-Murnaghan equation of state (EoS) (solid blue line) with B_0 = 249(3) GPa, B_0' = 4.0 (fixed) and calculated EoS (dashed lines) with B_0 (DFT-LDA) = 257 GPa, B_0' = 4.0 (fixed); B_0 (DFT-GGA) = 225 GPa, B_0' = 4.0 (fixed). Different colored symbols represent data points from six independent experimental runs.

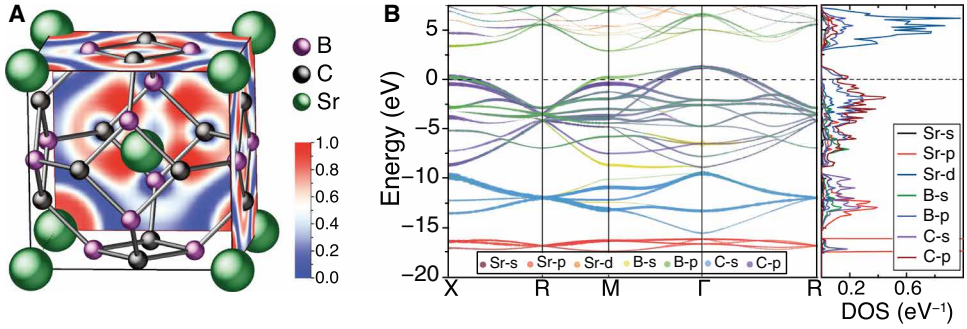

Fig. 4. Electronic properties of SrB_3C_3 at 0 GPaAB. (**A**) 2D electron localization function (ELF) for SrB_3C_3. The ELF indicates the probability of finding electrons in different regions of the crystal. Large ELF values (>0.6) indicate the formation of covalent bonds. (**B**) Electronic band structure for SrB_3C_3 projected onto atomic orbitals represented by different colors, where the width of each band is proportional to the weight of the corresponding orbital character. The projected density of states (DOS) in SrB_3C_3 is shown in the right. The Fermi energy is set to 0 eV (dashed line).

MATERIALS AND METHODS

Calculations

Structure-searching calculations were performed using the CALYPSO structure prediction method (*31*) based on the global minimization of free energy using ab initio total energy calculations. Structure searching simulations through CALYPSO code were performed in the Sr-B-C system (including pure elements, binaries, and ternaries from SrB_xC_y, with $0 \le x$ and $y \le 6$) from 0 to 200 GPa after broader searching in ternary B-C systems with a variety of metals including Li, Na, Mg, and Ca. Total energy calculations were performed in the framework of DFT within the Perdew-Burke-Ernzerhof (*38*) generalized gradient approximation as implemented in the VASP (Vienna Ab Initio Simulation Package) code (*39*). The projector-augmented wave (PAW) method (*40*) was adopted with the PAW potentials taken from the VASP library, where $4s^24p^65s^2$, $2s^22p^1$, and $2s^22p^2$ are treated as valence electrons for Sr, B, and C atoms, respectively. The use of a plane-wave kinetic energy cutoff of 520 eV and dense *k*-point sampling, adopted here, was shown to give excellent convergence of total energies. Electronic charges were calculated using a Bader charge analysis scheme using a 600 × 600 × 600 fast Fourier transform grid. Phonon dispersion calculations were performed to determine the dynamical stability of the predicted structures by using

the finite displacement approach, as implemented in the Phonopy code (*41*). The Vickers hardness (H_v) was estimated to be 24 GPa by using the empirical method proposed by Guo *et al.* (*42*).

Synthesis

Strontium metal was purified by sublimation (950°C, dynamic vacuum) onto Mo foil from a graphite crucible; graphite powder was pretreated at 950°C under dynamic vacuum for 16 hours to remove adsorbed species. Strontium carbide (SrC_2) was prepared by heating 2.780 g of Sr (31.7 mmol) with 0.371 g of graphite powder (30.9 mmol) in a capped graphite crucible under dynamic vacuum at 825°C for 16 hours. Excess Sr was subsequently sublimed at 950°C, and the resulting pale gray SrC_2 powder (1.400 g, 81% yield) was isolated from the crucible under Ar. Powder XRD showed a small SrO impurity. SrB_6 (EPSI Metals, 99.5%) and glassy carbon (Sigma-Aldrich, 99.95%) were purchased commercially and used without further purification. Binary (SrB_6 + $3SrC_2$) and ternary (SrB_6 + SrC_2 + 4C) mixtures were prepared under an inert Ar atmosphere, sealed, and then vigorously milled using Si_3N_4 media at 600 rpm for 1-min cycles over ~12 hours. The milled powders were removed from the media in an Ar glovebox, and thin plates (10 μm) were pressed between two diamond anvils with 1-mm culets and then loaded into DAC sample chambers using 100- to 300-μm culets and Re gaskets. Ne or alumina plates served as the pressure transmitting media and thermal insulation from the diamond anvils. After being compressed to the target pressure between 50 and 150 GPa, samples were heated to ~2500 K using the double-sided laser heating systems at High Pressure Collaborative Access Team (HPCAT) (*43*) or GeoSoilEnviro Center for Advanced Radiation Sources (GSECARS) (*44*). Temperatures near 3000 K were needed to produce crystalline grains with size comparable to the x-ray beam.

XRD and crystal structure determination

In situ powder XRD patterns were collected at the Advanced Photon Source, Sector 16, HPCAT, using a monochromatic wavelength of 0.4066 Å and at Sector 13, GSECARS, using a monochromatic wavelength of 0.3344 Å. The x-ray beam was focused on the sample, and scattered x-rays were detected using a PILATUS 1M or MarCCD detector. The sample-to-detector distance and geometrical parameters were calibrated using CeO_2 and LaB_6 standards with the DIOPTAS software (*45*). Pressure was calibrated using the equations of state of Ne and/or Al_2O_3 and cross-checked using the SrO equation of state and ruby fluorescence in some samples. Rietveld refinements of XRD patterns were conducted using PowderCell (*46*) and GSAS with EXPGUI (*47*).

Diffraction from crystalline grains suitable for analysis by multigrain crystallography methods were analyzed in the Fable package (*48*) with ImageD11 and GrainSpotter (*49*). Indexing and integration were performed using GSE_ADA/RSV (*50*), and the structure was solved using direct methods using SHELXS and refined using SHELXL-2014 (*51*) invoked within the Olex2 suite (*52*). A full description of the single-crystal diffraction analysis is provided in the Supplementary Materials. CSD 1949948 contains supplementary crystallographic data for this paper. These data can be obtained free of charge from the joint Cambridge Crystallographic Data Centre's and FIZ Karlsruhe's service to view and retrieve structures via www.ccdc.cam.ac.uk/structures/.

Scanning electron microscopy with energy-dispersive x-ray spectroscopy

Scanning electron microscopy (SEM) with energy-dispersive x-ray spectroscopy (EDS) was performed on a recovered sample using a JEOL 6500F field-emission scanning electron microscope equipped with an Oxford Instruments X-Max detector (80 mm^2). The laser-heated DAC sample was recovered from ~50 GPa after synchrotron XRD measurements, which verified the cubic powder diffraction pattern of SrB_3C_3. The Re gasket was placed onto an Al stub with carbon adhesive under the insert atmosphere of an Ar glovebox. The stub was sealed under Ar and transferred into the microscope by using a polyethylene glove bag that was sealed around the exchange chamber and purged with Ar. A beam of 15 keV and 1 nA was focused to a working distance of 10 mm, and an energy range of 10 keV was divided into 2048 channels for an energy resolution of ~5 eV. Aztec software developed by Oxford Instruments was used for EDS data analysis.

SUPPLEMENTARY MATERIALS

Supplementary material for this article is available at http://advances.sciencemag.org/cgi/content/full/6/2/eaay8361/DC1

Single-crystal diffraction analysis

Fig. S1. Stability of SrB_3C_3 and analysis of different possible stoichiometries.

Fig. S2. SEM and EDS measurements.

Fig. S3. Raw XRD patterns.

Fig. S4. Sr-B-C phase identification.

Fig. S5. Optical images of SrB_3C_3 during synthesis near 50 GPa.

Fig. S6. Electronic structures for SrB_3C_3.

Fig. S7. Phonon dispersion curves and energetic stabilities as a function of pressure.

Fig. S8. Fourier difference map (F_{obs}-F_{calc}) from single-crystal analysis.

Table S1. Comparison of single-crystal diffraction refinement quality indicators for different "colorings" of clathrate framework in crystal structure models of the SrB_3C_3 clathrate.

Table S2. Calculated Bader partial charges of the SrB_3C_3 clathrate at 0 GPa.

Table S3. Calculated structural parameters of Sr-B-C phases.

Table S4. SrB_3C_3 lattice parameters during decompression.

Data file S1. CIF file of the single-crystal XRD data and the best model of the crystal structure for the SrB_3C_3 clathrate.

REFERENCES AND NOTES

1. Y. Cao, V. Fatemi, S. Fang, K. Watanabe, T. Taniguchi, E. Kaxiras, P. Jarillo-Herrero, Unconventional superconductivity in magic-angle graphene superlattices. *Nature* **556**, 43–50 (2018).
2. J. Akimitsu, K. Takenawa, K. Suzuki, H. Harima, Y. Kuramoto, High-temperature ferromagnetism in CaB_2C_2. *Science* **293**, 1125–1127 (2001).
3. M. Worle, R. Nesper, G. Mair, M. Schwarz, H. G. Von Schnering, LiBC–A completely intercalated heterographite. *Z. Anorg. Allg. Chem.* **621**, 1153–1159 (1995).
4. X. Rocquefelte, S. E. Boulfelfel, M. B. Yahia, J. Bauer, J. Y. Saillard, J. F. Halet, Structural preference versus metal within the MB2C2 (M=Mg, Sc, Ca, Y, Ln) Phases: The coloring problem revisited by DFT calculations. *Angew. Chemie. Int. Ed. Engl.* **44**, 7542–7545 (2005).
5. C. Frondel, U. B. Marvin, Lonsdaleite, a hexagonal polymorph of diamond. *Nature* **214**, 587–589 (1967).
6. V. L. Solozhenko, O. O. Kurakevych, D. Andrault, Y. Le Godec, M. Mezouar, Ultimate metastable solubility of boron in diamond: Synthesis of superhard diamondlike BC_5. *Phys. Rev. Lett.* **102**, 015506 (2009).
7. C. L. Burdick, E. A. Owen, The atomic structure of carborundum determined by X-rays. *J. Am. Chem. Soc.* **40**, 1749–1759 (1918).
8. V. L. Solozhenko, D. Andrault, G. Fiquet, M. Mezouar, D. C. Rubie, Synthesis of superhard cubic BC_2N. *Appl. Phys. Lett.* **78**, 1385–1387 (2001).
9. H. K. Clark, J. L. Hoard, The crystal structure of boron carbide. *J. Am. Chem. Soc.* **65**, 2115–2119 (1943).
10. Q. An, W. A. Goddard III, T. Cheng, Atomistic explanation of shear-induced amorphous band formation in boron carbide. *Phys. Rev. Lett.* **113**, 095501 (2014).
11. H. M. El-Kaderi, J. R. Hunt, J. L. Mendoza-Cortés, A. P. Côté, R. E. Taylor, M. O'Keeffe, O. M. Yaghi, Designed synthesis of 3D covalent organic frameworks. *Science* **316**, 268–273 (2007).
12. R. Hoffmann, A. A. Kabanov, A. A. Golov, D. M. Proserpio, Homo citans and carbon allotropes: For an ethics of citation. *Angew. Chem. Int. Ed.* **55**, 10962–10976 (2016).
13. D. M. Teter, R. J. Hemley, Low-compressibility carbon nitrides. *Science* **271**, 53–55 (1996).
14. C. S. Yoo, H. Cynn, F. Gygi, G. Galli, V. Iota, M. Nicol, S. Carlson, D. Häusermann, C. Mailhiot, Crystal structure of carbon dioxide at high pressure: "Superhard" polymeric carbon dioxide. *Phys. Rev. Lett.* **83**, 5527–5530 (1999).

15. G. S. Nolas, J. L. Cohn, G. A. Slack, S. B. Schujman, Semiconducting Ge clathrates: Promising candidates for thermoelectric applications. *Appl. Phys. Lett.* **73**, 178–180 (1998).
16. M. Beekman, G. S. Nolas, Inorganic clathrate-II materials of group 14: Synthetic routes and physical properties. *J. Mater. Chem.* **18**, 842–851 (2008).
17. C. Baerlocher, L. B. McCusker, D. H. Olson, *Atlas of Zeolite Framework Types* (Elsevier Science, 2007).
18. J. S. Kasper, P. Hagenmuller, M. Pouchard, C. Cros, Clathrate structure of silicon Na_8Si_{46} and Na_xSi_{136} (x < 11). *Science* **150**, 1713–1714 (1965).
19. C. Cros, M. Pouchard, P. Hagenmuller, Sur deux nouvelles phases du systeme silicium-sodium. *C. R. Acad. Sci.* **260**, 4764–4767 (1965).
20. R. Nesper, K. Vogel, P. E. Blöchl, Hypothetical carbon modifications derived from zeolite frameworks. *Angew. Chem. Int. Ed.* **32**, 701–703 (1993).
21. A. J. Karttunen, T. F. Fässler, M. Linnolahti, T. A. Pakkanen, Structural principles of semiconducting group 14 clathrate frameworks. *Inorg. Chem.* **50**, 1733–1742 (2011).
22. X. Blase, P. Gillet, A. San Miguel, P. Mélinon, Exceptional ideal strength of carbon clathrates. *Phys. Rev. Lett.* **92**, 215505 (2004).
23. I. Spagnolatti, M. Bernasconi, G. Benedek, Electron-phonon interaction in carbon clathrate hex-C_{40}. *Euro. Phys. J. B* **34**, 63–67 (2003).
24. X. Blase, E. Bustarret, C. Chapelier, T. Klein, C. Marcenat, Superconducting group-IV semiconductors. *Nat. Mater.* **8**, 375–382 (2009).
25. M. Bernasconi, S. Gaito, G. Benedek, Clathrates as effective p-type and n-type tetrahedral carbon semiconductors. *Phys. Rev. B* **61**, 12689–12692 (2000).
26. N. Rey, A. Muñoz, P. Rodríguez-Hernández, A. San Miguel, First-principles study of lithium-doped carbon clathrates under pressure. *J. Phys. Cond. Mat.* **20**, 215218 (2008).
27. S. Yamanaka, A. Kubo, N. S. Kini, K. Inumaru, An attempt to prepare carbon clathrate compounds using high-pressure and high-temperature conditions. *Physica B* **383**, 59–62 (2006).
28. T. L. Heying, J. W. Ager Jr., S. L. Clark, D. J. Mangold, H. L. Goldstein, M. Hillman, R. J. Polak, J. W. Szymanski, A new series of organoboranes. I. Carboranes from the reaction of decaborane with acetylenic compounds. *Inorg. Chem.* **2**, 1089–1092 (1963).
29. R. N. Grimes, *Carboranes* (Elsevier Science, 2016).
30. T. Zeng, R. Hoffmann, R. Nesper, N. W. Ashcroft, T. A. Strobel, D. M. Proserpio, Li-Filled, B-substituted carbon clathrates. *J. Am. Chem. Soc.* **137**, 12639–12652 (2015).
31. Y. Wang, J. Lv, L. Zhu, Y. Ma, Crystal structure prediction via particle-swarm optimization. *Phys. Rev. B* **82**, 094116 (2010).
32. A. S. Mikhaylushkin, X. Zhang, A. Zunger, Crystal structures and metastability of carbon-boron compounds C_3B and C_5B. *Phys. Rev. B* **87**, 094103 (2013).
33. V. H. Bode, G. Teufer, Die Kristallstruktur der Hexafluorophosphorsäure. *Acta Crystallogr.* **8**, 611–614 (1955).
34. X. Liang, A. Bergara, L. Wang, B. Wen, Z. Zhao, X.-F. Zhou, J. He, G. Gao, Y. Tian, Potential high-T_c superconductivity in $CaYH_{12}$ under pressure. *Phys. Rev. B* **99**, 100505 (2019).
35. J. H. Westbrook, H. Conrad, *The Science of Hardness Testing and Its Research Applications* (American Society for Metals, 1973).
36. A. Simon, Superconductivity and chemistry. *Angew. Chemie. Int. Ed. Engl.* **36**, 1788–1806 (1997).
37. D. Y. Kim, S. Stefanoski, O. O. Kurakevych, T. A. Strobel, Synthesis of an open-framework allotrope of silicon. *Nat. Mater.* **14**, 169–173 (2015).
38. J. P. Perdew, Y. Wang, Accurate and simple analytic representation of the electron-gas correlation energy. *Phys. Rev. B* **45**, 13244–13249 (1992).
39. G. Kresse, J. Furthmüller, Efficient iterative schemes for ab initio total-energy calculations using a plane-wave basis set. *Phys. Rev. B* **54**, 11169–11186 (1996).
40. P. E. Blöchl, Projector augmented-wave method. *Phys. Rev. B* **50**, 17953–17979 (1994).
41. A. Togo, F. Oba, I. Tanaka, First-principles calculations of the ferroelastic transition between rutile-type and $CaCl_2$-type SiO_2 at high pressures. *Phys. Rev. B* **78**, 134106 (2008).
42. X. Guo, L. Li, Z. Liu, D. Yu, J. He, R. Liu, B. Xu, Y. Tian, H.-T. Wang, Hardness of covalent compounds: Roles of metallic component and d valence electrons. *J. Appl. Phys.* **104**, 023503 (2008).
43. Y. Meng, R. Hrubiak, E. Rod, R. Boehler, G. Shen, New developments in laser-heated diamond anvil cell with in situ synchrotron x-ray diffraction at High Pressure Collaborative Access Team. *Rev. Sci. Instrum.* **86**, 072201 (2015).
44. V. B. Prakapenka, A. Kubo, A. Kuznetsov, A. Laskin, O. Shkurikhin, P. Dera, M. L. Rivers, S. R. Sutton, Advanced flat top laser heating system for high pressure research at GSECARS: Application to the melting behavior of germanium. *High Press. Res.* **28**, 225–235 (2008).
45. C. Prescher, V. B. Prakapenka, DIOPTAS: A program for reduction of two-dimensional X-ray diffraction data and data exploration. *High Press. Res.* **35**, 223–230 (2015).
46. W. Kraus, G. Nolze, POWDER CELL-A program for the representation and manipulation of crystal structure and calculation of the resulting X-ray powder pattern. *J. Appl. Cryst.* **29**, 301–303 (1996).
47. B. H. Toby, EXPGUI, a graphical user interface for GSAS. *J. Appl. Cryst.* **34**, 210–213 (2001).
48. H. O. Sørensen, S. Schmidt, J. P. Wright, G. B. M. Vaughan, S. Techert, E. F. Garman, J. Oddershede, J. Davaasambuu, K. S. Paithankar, C. Gundlach, H. F. Poulsen, Multigrain crystallography. *Z. Kristallogr.* **227**, 63–78 (2011).
49. S. Schmidt, GrainSpotter: A fast and robust polycrystalline indexing algorithm. *J. Appl. Cryst.* **47**, 276–284 (2014).
50. P. Dera, K. Zhuravlev, V. Prakapenka, M. L. Rivers, G. J. Finkelstein, O. Grubor-Urosevic, O. Tschauner, S. M. Clark, R. T. Downs, High pressure single-crystal micro X-ray diffraction analysis with GSE_ADA/RSV software. *High Press. Res.* **33**, 466–484 (2013).
51. G. M. Sheldrick, Crystal structure refinement with SHELXL. *Acta Crystallogr. C Struct. Chem.* **71**, 3–8 (2015).
52. O. V. Dolomanov, L. J. Bourhis, R. J. Gildea, J. A. K. Howard, H. Puschmann, OLEX2: A complete structure solution, refinement and analysis program. *J. Appl. Cryst.* **42**, 339–341 (2009).

Acknowledgments: We are grateful to R. Hoffmann for providing inspiration and guidance for this work. We thank A. Karandikar, V. Bhadram, and R. Hrubiak for assistance with experiments and T. Zeng and R. Nesper for insightful comments. **Funding:** This work was supported by DARPA under grant no. W31P4Q1310005. Additional support was provided by the Energy Frontier Research in Extreme Environments (EFree) Center, an Energy Frontier Research Center funded by the U.S. Department of Energy, Office of Science under award no. DE-SC0001057. P.A.G. thanks Polish National Agency for Academic Exchange and Warsaw University of Technology for financial support. Computations were conducted using the supercomputer Copper of DoD HPCMP Open Research Systems under project no. ACOMM35963RC1 and the Memex cluster of Carnegie Institution for Science. R.E.C. was also supported by the European Research Council Advanced Grant ToMCaT. Portions of this work were performed at HPCAT (Sector 16) and GeoSoilEnviroCARS (The University of Chicago, Sector 13), Advanced Photon Source (APS), Argonne National Laboratory. HPCAT operations are supported by DOE-NNSA's Office of Experimental Sciences. GeoSoilEnviroCARS is supported by the NSF—Earth Sciences (EAR-1634415) and Department of Energy—GeoSciences (DE-FG02-94ER14466). The Advanced Photon Source is a U.S. Department of Energy (DOE) Office of Science User Facility operated for the DOE Office of Science by Argonne National Laboratory under contract no. DE-AC02-06CH11357. **Author contributions:** L.Z. and H.L. performed the calculations, and L.Z., H.L., and R.E.C. contributed to the computational analyses. G.M.B., M.G., J.-A.D., P.A.G., Y.M., E.G., V.B.P., B.L.C., A.E., and T.A.S. performed the experiments. P.A.G. and T.A.S. analyzed XRD data for multiple single crystalline grains. All authors analyzed the data, discussed the results, and contributed to writing the manuscript. **Competing interests:** T.A.S. and L.Z. are inventors on a provisional patent application related to this work filed by Carnegie Institution of Washington (U.S. Serial No. 62,814,024, filed 5 March 2019). The authors declare that they have no other competing interests. **Data and materials availability:** All data needed to evaluate the conclusions in the paper are present in the paper and/or the Supplementary Materials. Additional data related to this paper may be requested from the authors.

Submitted 22 July 2019
Accepted 13 November 2019
Published 10 January 2020
10.1126/sciadv.aay8361

Citation: L. Zhu, G. M. Borstad, H. Liu, P. A. Guńka, M. Guerette, J.-A. Dolyniuk, Y. Meng, E. Greenberg, V. B. Prakapenka, B. L. Chaloux, A. Epshteyn, R. E. Cohen, T. A. Strobel, Carbon-boron clathrates as a new class of sp^3-bonded framework materials. *Sci. Adv.* **6**, eaay8361 (2020).